ACS NANO

www.acsnano.org

ARTICLE

Slowing DNA Translocation in a Nanofluidic Field-Effect Transistor

Yifan Liu[†] and Levent Yobas*[,†,‡]

[†]Department of Electronic and Computer Engineering, [‡]Division of Biomedical Engineering, The Hong Kong University of Science and Technology, Clear Water Bay, Kowloon, Hong Kong S. A. R.

Supporting Information

ABSTRACT: **Here, we present an experimental demonstration of slowing DNA translocation across a nanochannel by modulating the channel surface charge through an externally applied gate bias. The experiments were performed on a nanofluidic field-effect transistor, which is a monolithic integrated platform featuring a 50 nm-diameter in-plane alumina nanocapillary whose entire length is surrounded by a gate electrode. The field-effect transistor behavior was validated on the gating of ionic conductance and protein transport. The gating of DNA translocation was subsequently studied by measuring discrete current dips associated with single λ-DNA translocation events under a source-to-drain bias of 1 V. The translocation speeds under various gate bias conditions were extracted by fitting event histograms of the measured translocation time to the first passage time distributions obtained from a simple 1D biased diffusion model. A positive gate bias was observed to slow the translocation of single λ-DNA chains markedly; the translocation speed was reduced by an order of magnitude from 18.4 mm/s obtained under a floating gate down to 1.33 mm/s under a positive gate bias of 9 V. Therefore, a dynamic and flexible regulation of the DNA translocation speed, which is vital for single-molecule sequencing, can be achieved on this device by simply tuning the gate bias. The device is realized in a conventional semiconductor microfabrication process without the requirement of advanced lithography, and can be potentially further developed into a compact electronic single-molecule sequencer.**

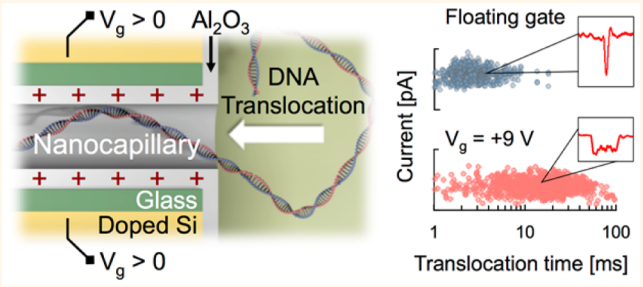

KEYWORDS: *nanofluidic transistor, DNA, nanochannel, field-effect, nanopore sequencing*

In recent years, nanopores and nanochannels have been extensively used in the area of single-molecule analysis[1,2] for practical applications including protein/DNA detection,[3−5] genome mapping,[6,7] and DNA sequencing.[8] Among those, nanopore-based DNA sequencing is being considered as a revolutionary next-generation technique because of its potential toward a high-throughput affordable sequencing.[9] In this technique, a single DNA chain is driven through a nanopore electrophoretically while the corresponding fluctuations in ionic or transverse tunneling current are being monitored to discern nucleotide bases crossing the nanopore. However, a key challenge faced in this technique is that the DNA chain crosses the nanopore extremely rapidly, which prevents the sequence from being discerned at single-base resolution.[10] Although scientists have explored the utility of integrated sensors featuring high intrinsic speeds for nanopores (*e.g.*, a nanowire field-effect transistor integrated with a nanopore),[11] the DNA chain translocation must be slowed in order to relax the bandwidth requirement imposed on the sensing electronics. This can be achieved by lowering the driving electric field but at the expense of sensing current strength and signal-to-noise ratio. Moreover, if an excessively low field is applied, the DNA chain might be prevented from entering the nanopore by an existing entropic energy barrier.

An assortment of methods have been reported for reducing the DNA translocation speed, which may involve lowering the temperature,[12] tuning the salt concentration,[13] increasing the solvent viscosity,[12] or functionalizing the surface for enhanced DNA−surface interactions.[14] Although such passive techniques can slow the motion of DNA through the nanopore to a certain extent, they do not allow active modulation of the translocation process. Trepagnier *et al.* demonstrated an ingenious method of slowing DNA translocation through artificial nanopores by using optical tweezers.[15] However, this method requires carefully focusing a laser beam on a microsphere attached to the DNA chain for effective manipulation. Tsutsui *et al.* reported a label-free electrical strategy by applying a transverse electric field through nanogap electrodes across a nanochannel, but this led to the issue of crosstalk between ionic and

Received: January 25, 2016
Accepted: March 28, 2016
Published: March 28, 2016

DOI: 10.1021/acsnano.6b00610
ACS Nano 2016, 10, 3985−3994

transverse currents.[16] An active and effective label-free method of slowing DNA translocation is still a remaining challenge.

Theoretical studies[17−19] have predicted that DNA movement in a nanopore/channel can be slowed by electrically modulating the wall surface charge, based on a careful analysis of the induced electroosmotic flow (EOF) and DNA−nanopore/channel electrostatic interactions. Such theoretical studies are largely inspired by the recent demonstration of nanofluidic field-effect transistor (NFET) that is a nanofluidic platform in which a gate electrode is integrated around a nanopore/channel for electrically modulating the surface charge of the dielectric walls. NFET is pioneered by Karnik *et al.*, who developed an integrated device featuring a metal gate electrode patterned on top of a planar 30 nm slit formed by etching a sacrificial layer, and demonstrated its use in controlling the ionic conductance and the transport of avidin.[20,21] Subsequent efforts have been directed toward a more efficient field-effect modulation by using structures featuring 2D confinement (*e.g.*, nanochannels and nanopores) and more effective gate electrode configurations (*e.g.*, an all-around gate).[22,23] Prominent examples include electrode-embedded multiple nanopores fabricated on Si_3N_4 membranes[24] and in-plane circular alumina nanochannels covered by gate electrodes built on silicon substrates.[25] However, despite the theoretical predictions, practical usefulness of these powerful nanofluidic devices in reducing the DNA translocation speed has been rarely explored; Paik *et al.* demonstrated a gated nanopore array for manipulating DNA but rather investigated the DNA capture rate of the nanopore array under a gate bias.[26]

For reducing the DNA translocation speed in nanopore sequencing, a nanopore-based NFET appears to be a natural choice. However, a high aspect ratio structure imposing extensive confinement can accommodate and stretch DNA over its entire length; thus, a profound field-effect regulation of the translocation event is likely to arise from a nanochannel-based NFET owing to enhanced DNA−surface interactions.[27−29] Moreover, nanochannels, if they could be made with a diameter far below the persistence length, would enhance the energetic cost of DNA existing in a folded state, thus ensuring a kink-free translocation of a stretched chain.[28] Such folded conformation often arises in nanopore experiments due to a thermal-induced bending of the chain[30] and poses a further impediment to sequencing. Furthermore, given their in-plane configuration, nanochannels enable a real-time optical probing of the chain concomitant with electrical measurements. Unlike nanopores, which are typically positioned out-of-plane on a thin membrane, in-plane nanochannels are less cumbersome in fluidic isolation, *i.e.*, nanochannels and fluidic access channels can be integrated onto a surface and readily encapsulated from above all at once.[31] This allows for a high-density array for a massively parallel sequencing when coupled with tunneling electrodes or in-plane nanoconstrictions.[28] However, the fabrication of such nanochannels relies on time-consuming sacrificial etching[21] or low-throughput advanced lithography,[22,25] which might limit their potential in practical use.

In this study, we present an experimental demonstration of slowing DNA translation through a nanochannel by modulating the channel surface charge under an external gate bias. Figure 1a describes the concept where a DNA coil is illustrated being electrophoretically driven into the nanochannel and stretched therein under confinement. During this process, pronounced electrostatic interactions occur between the DNA chain and the

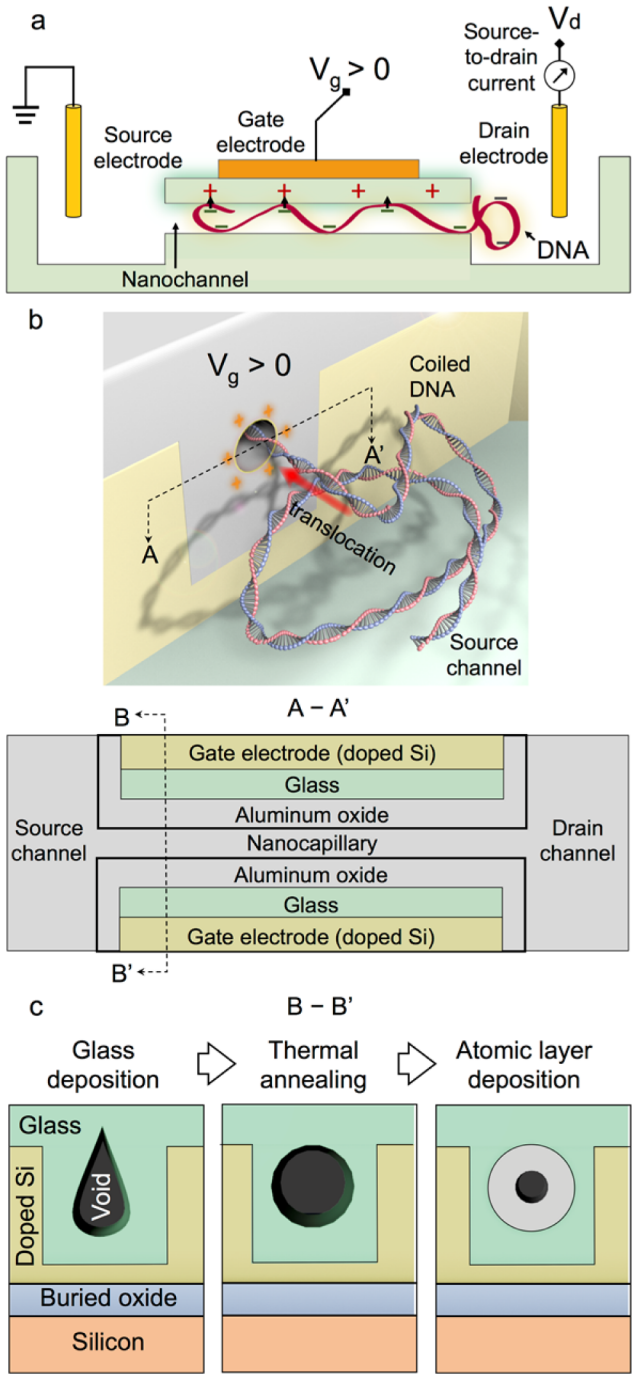

Figure 1. Illustrations: (a) the concept of slowing DNA translocation through a nanochannel under an external gate bias; (b) the nanocapillary-based NFET structure introduced here; and (c) key process steps. (a) The translocation speed can be lowered by the electrostatic interactions with an induced surface charge under a positive gate bias ($V_g > 0$). (b) Upper panel: A 3D rendering of the nanocapillary opening viewed from source channel. Lower panel: longitudinal section (A−A′) of the glass nanocapillary viewed from above illustrating the surrounding layers including the bulk gate electrode (doped Si). (c) Cross section (B−B′) viewed after key process steps illustrating a void self-enclosed within a trench due to nonconformal glass deposition, the subsequent shape transformation of the void into a cylindrical tube during the thermal reflow step, and the further narrowing of the tube during the atomic layer deposition step of Al_2O_3. The nanocapillary is built into the device layer of a SOI wafer, which is heavily doped and thus can serve as a gate electrode.

DOI: 10.1021/acsnano.6b00610
ACS Nano 2016, 10, 3985−3994

channel wall, which is strongly positively charged owing to a positive gate bias. To assess the effectiveness of such interactions in slowing the DNA chain, we developed a monolithic integrated NFET device featuring a 50 nm-diameter high aspect-ratio (micrometers-long) in-plane alumina nanocapillary whose entire length is surrounded by a gate electrode (Figure 1b). Notably, the nanocapillary is realized through a facile process that exploits the thermal reflow of a doped glass layer within a micrometer-scale trench etched directly into a bulk gate electrode layer. Specifically, a buried void inside the trench is transformed into a cylindrical tube[32−34] and the tube is further scaled down by atomic layer deposition (ALD) of Al_2O_3 after creating fluidic access channels (Figure 1c); therefore, high-resolution advanced lithography is not required. The cost-effective and robust platform demonstrated herein can potentially be integrated with a nanopore sensor for developing a sensitive and affordable sequencing system.

RESULTS AND DISCUSSION

Device Structure. Figure 2a illustrates the overall integrated device in which fluidic microchannels "source" and

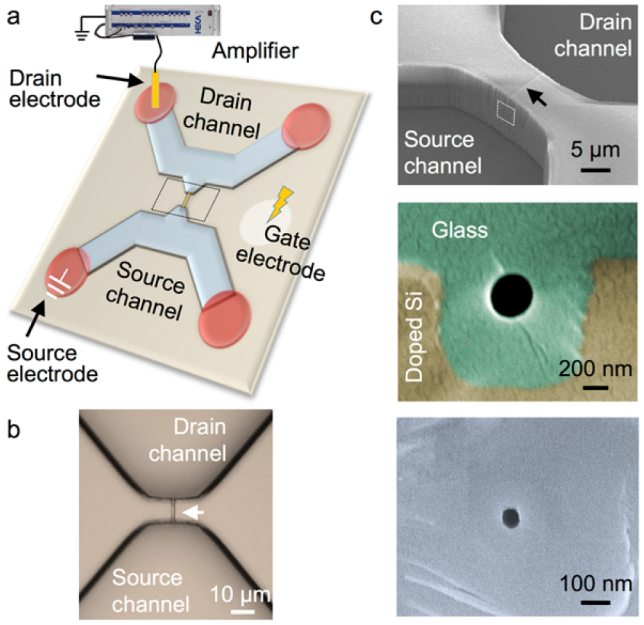

Figure 2. (a) A rendering of the nanocapillary-based NFET illustrating electrical connections during active transport. The dashed rectangle highlights the nanocapillary that is further depicted in an (b) optical micrograph and in (c) SEM images. (c) The oblique view of the source-drain partition (upper panel) was captured before the atomic layer deposition step. The capillary entrance (the dashed rectangle) is further detailed in a subsequent image (middle panel), in which pseudo coloring is used to denote the glass layer (green) and the doped silicon layer (yellow). The capillary diameter is ∼300 nm as a result of the thermal reflow of doped glass, and is further narrowed to ∼50 nm by the atomic layer deposition of Al_2O_3 (lower panel). The arrows in (b) and (c) mark the position of the nanocapillary.

"drain" are created on a silicon-on-insulator (SOI) substrate by entirely removing the device layer from patterned regions. The two microchannels are connected through an in-plane nanocapillary fabricated inside a 1-μm-wide and -deep trench formed within a heavily doped 4.5-μm-thick silicon device layer, which serves as the gate electrode. Figure 2b shows an optical micrograph of a representative device, closing on the 10-μm-long nanocapillary, whereas Figure 2c shows a scanning electron microscopy (SEM) image depicting the source-drain partition where the nanocapillary is situated (arrow). Figure 2c also displays close-up SEM images of the capillary opening before and after Al_2O_3 deposition. As can be seen, the capillary opening exhibits a round profile that is ∼300 nm in diameter as a result of the thermal reflow of doped glass. This profile is maintained during the subsequent alumina deposition step that further scaled the capillary diameter down to ∼50 nm. Each fabricated device was bonded with a cover slab of polydimethylsiloxane (PDMS) featuring access ports after surface activation in oxygen plasma. The detailed fabrication process, and further SEM images are provided in Supporting Information (Figures S1 and S2).

Device Characteristics. The fabricated NFET was first characterized for the ionic transport properties under a floating gate voltage (V_g). Figure 3a displays the ionic conductance of the nanocapillaries (G_c) as a function of KCl concentration (C_{KCl}) from representative devices featuring two distinct capillary lengths (l = 10 and 20 μm). The results show that the ionic conductance depends linearly on C_{KCl} in the high-salt regime (>0.01 M), which suggests that G_c is primarily dominated by the bulk conductivity. A conductance plateau is observed in the low-salt regime ($C_{KCl} \leq 0.01$ M), which indicates that G_c is mostly independent of the bulk ionic strength in both devices. This behavior suggests a surface-charge-governed ionic transport property, which is associated with increasingly thicker electrical double layers (EDLs) at reduced salt concentrations. The surface charge density of the nanocapillary was predicted as σ = 8 mC/m^2 by fitting the measured ionic conductance values to a theoretical model (solid and dashed lines) that accounts for the surface-charge-governed conductance in addition to the bulk conductance (Supporting Information). This is close to the value reported for Al_2O_3 as 10 mC/m^2 at neutral pH.[35] We also investigated the impact of pH on the ionic conductance of the nanocapillary (l = 10 μm) at fixed KCl concentrations (inset in Figure 3a). At a high KCl concentration (C_{KCl} = 0.1 M), no marked variation was observed over a broad pH range (3−11) and the ionic conductance was almost constant (∼230 pS), which suggests that the surface charge contributes little to the ionic conductance under this particular electrolyte condition (the Debye length, $\lambda_D \sim 1$ nm). The conductance is dominated by the bulk ionic concentration. However, the pH substantially affected the ionic conductance at a low ionic strength (C_{KCl} = 0.1 mM) where the Debye length ($\lambda_D \sim 33$ nm) is comparable to the size of the capillary opening (*i.e.*, overlapping EDLs), which confirms that the ionic conductance is governed predominantly by the surface charge at the stated ionic strength. The comparatively low ionic conductance observed at pH 7 and 9 indicates an overly suppressed surface charge of the nanocapillary in this pH range, which coincides with the isoelectric point (pI) of alumina reported in the literature (pI ∼ 8).[35]

These results concur with previous theoretical studies predicting the pH and salt concentration dependence characteristics of ionic conductance in a nanochannel/pore.[36−38] Moreover, the results rule out potential leakage pathways and further confirm that the measurements originate from the ionic current through the nanocapillary. The aforementioned studies concluded that the ionic conductance of a nanochannel at low ionic strengths (thick EDL) is largely dependent on the

DOI: 10.1021/acsnano.6b00610
ACS Nano 2016, 10, 3985−3994

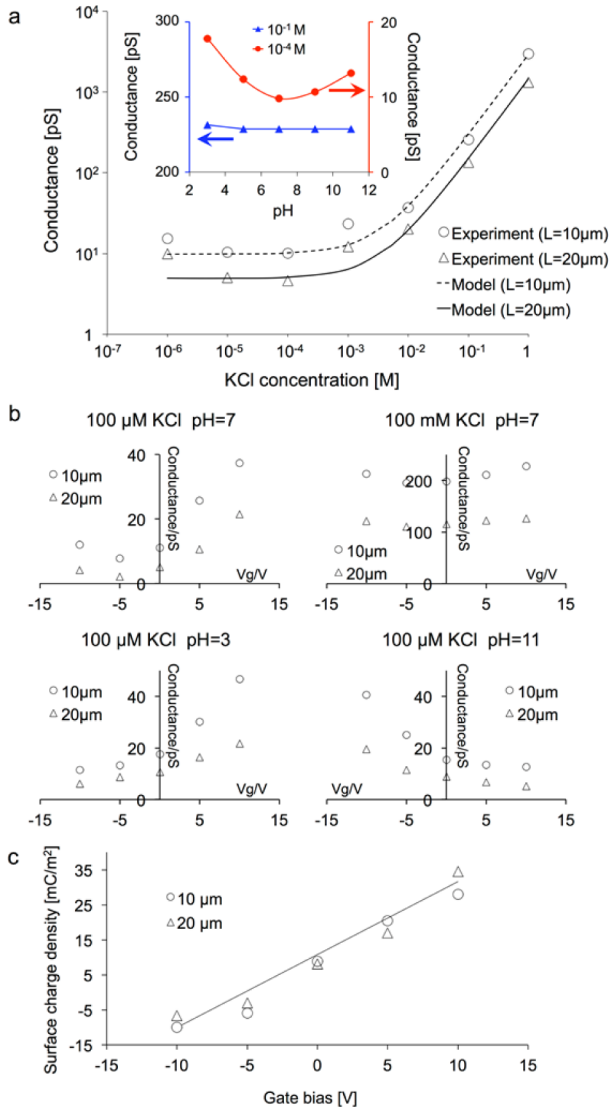

Figure 3. Device characteristics. (a) Measured ionic conductance plotted as a function of KCl concentration for representative devices featuring two distinct capillary lengths (legend) and shown with respective curves describing theoretical predictions all obtained with a floating gate electrode. The inset shows the pH dependence of the ionic conductance measured through the 10-μm-long nanocapillary for two ionic strengths (10^{-4} and 10^{-1} M KCl). Field-effect modulation: (b) ionic conductance ($G_c - V_g$) measured under various electrolyte conditions; (c) surface charge density ($\sigma - V_g$) predicted based on the theoretical fitting of the measured ionic conductance for the case of 10^{-4} M KCl and pH 7.

solution pH, which is explained by the charge-regulated nature of the dielectric nanochannel materials in contact with aqueous solution and the surface-charge-governed ionic transport behavior. As the dielectric surface carries reactive groups, MOH, where M denotes the particular oxide type (*e.g.*, Al), the charge property of the surface groups is determined by the local hydrogen ion concentration according to the dissociation reactions: $MOH \leftrightarrow MO^- + H^+$ and $MOH_2^+ \leftrightarrow MOH + H^+$. Lowering (elevating) the solution pH increases (reduces) the local H^+ concentration in the nanocapillary, which then leads to enhanced chemical surface charge density with the reactive groups becoming increasingly protonated (deprotonated). Subsequently, the increased surface charge is screened by excess mobile counterions responsible for the charging of EDL and hence the rising of conductance.

The NFET was further characterized for the field-effect modulation of conductance under various electrolyte conditions ($G_c - V_g$ plots, Figure 3b). The ionic conductance G_c was derived from the respective sets of current–voltage ($I_d - V_d$) characteristics measured under distinct gate voltages (Supporting Information, Figure S3). As shown in the upper left panel, the application of a gate bias led to an effective modulation of the ionic conductance, with an ambipolar behavior being observed under the electrolyte condition of 100 μM KCl at neutral pH. On the basis of the theoretical fitting of the measured ionic conductance, σ was estimated as +28 and −10 mC/m^2 for V_g = +10 and −10 V, respectively (Figure 3c). This suggests that not only can the surface charge density of the nanocapillary be effectively modulated by the gate bias but also the polarity of its surface charge can be reversed. The ambipolar behavior arises from the comparatively low surface charge of alumina and effective gate modulation of our device. The latter also attests to the effective gate modulation of the zeta potential at low salt concentrations.[39] As expected, the modulation effect became negligible at a high salt concentration (C_{KCl} = 100 mM, upper right panel, Figure 3b) because the ionic transport was no longer surface-charge governed due to very thin EDLs in relation to the capillary diameter (Figure 3a). We also determined that the modulation behavior was pH-sensitive: under highly acidic (pH = 3, lower left panel) and alkaline (pH = 11, lower right panel) conditions, the devices exhibited a unipolar modulation behavior with opposite polarities. At pH 3 (pH 11), G_c increased (decreased) monotonically with the increase of V_g. This unipolar behavior resulted from the strong positive (negative) charge of alumina surface under the stated acidic (alkaline) condition as a result of the association–dissociation of the surface hydroxyl groups,[38] which cannot be completely quenched by the application of a negative (positive) gate bias. The device insulation was found adequate as the gate leakage currents were measured to be over an order of magnitude lower than the drain currents (Figure S4). The pH-sensitive gating behavior of the nanopore conductance has been also predicted in previous theoretical studies considering practical effects such as overlapping EDLs, Stern layer, EOF, and site dissociation/association reactions of the pore surface.[39−41]

Briefly, the underlying principle can be summarized based on the surface reactive groups and their ability to provide chemical buffering.[41] Under a floating gate, such groups are partially ionized depending on the solution pH and can modulate the chemical surface charge density by shifting their equilibrium, thereby compensating for the field effect under a specific gate bias. With an increased gate bias, the chemically reactive surface resists rapid changes in the EDL until all the surface groups become either completely ionized or completely neutralized. This is revealed in the conductance plots corresponding to the solution pH 3 and 7 (pH 11) under a negative (positive) gate bias where the rather poor sensitivity to the gating arises from chemical buffering of the positively (negatively) charged groups that are not fully saturated. When fully saturated, the screening of any additional gate bias occurs only through the EDL charging, which then leads to an increase in conductance. Here, this can be observed for the solution pH 7 (around −10 V gate), but not for pH 3 and 11, within the applied gate bias range because pH 7 is very close to pI of alumina where a comparatively small change in the gate bias can drive the

DOI: 10.1021/acsnano.6b00610
ACS Nano 2016, 10, 3985−3994

chemical surface charge density into a rapid saturation.[35] Under a gate bias of opposite polarity (positive for pH 3 and 7 and negative for pH 11), however, the surface groups become quickly neutralized (no chemical buffering), and thus, the EDL charging begins to screen the gate bias at a reduced bias strength, hence, the enhanced sensitivity of conductance to gating in this range. For a given gate bias, the conductance values at pH 3 are typically higher than those at pH 7 because the solution ionic strength increases with an increased deviation from neutral pH. At high salt, a thin EDL presents a relatively large differential capacitance, and thus, most of the applied gate bias falls across the dielectric wall capacitance, leaving only a small fraction for the EDL charging and, hence, the insensitivity of conductance to gating at high salt.

Field-Effect Control of Protein Transport. Before exploring the NFET for slowing the DNA translocation process, its field-effect capacity was further put to the test on the control of protein transport including enrichment, depletion and gated diffusive transport of proteins. We chose two proteins: GFP (pI ~ 6) and the lectin LcH (FITC-labeled, pI > 8). The proteins were diluted to a concentration of ~10 μM in 0.01× phosphate-buffered saline (PBS) at a low ionic strength (~1.6 mM) and neutral pH (7.4). At this pH, GFP and the lectin are negatively and positively charged, respectively. We used devices containing a 10-μm-long nanocapillary, and we filled both of the microchannels with the protein solution. The source and drain electrodes were held at a ground potential, and the gate terminal was fixed at a designated voltage. Figure 4a shows the results of representative GFP experiments obtained under three distinct gate voltages. The fluorescence emission was detectable but dim in the nanocapillary under a floating gate ($V_g \sim 0$). However, when a gate bias of +10 V was applied, the fluorescence intensity in the capillary increased substantially; this is because a positive gate bias renders the capillary surface strongly positive, which raises the electrostatic potential within the overlapped double layers and enriches the counter-charged GFP within the capillary. Conversely, under a negative gate bias, −10 V, the fluorescence in the nanocapillary was decreased to the levels indistinguishable from the background, which suggests that the surface charge became negative and consequently the GFP molecules were electrostatically repelled and excluded from the nanocapillary. The results of both the lectin and the GFP experiments were quantified for comparison by measuring the average fluorescence intensity in the nanocapillary regions (Figure 4b). The plot reveals that the modulation of the lectin concentration showed an opposite tendency to that of GFP; the lectin molecules were gradually enriched (enhanced fluorescence intensity) under an increased negative gate bias, whereas they were depleted (reduced fluorescence intensity) under a positive gate bias. These results verify the capacity of our transistor to control the concentration of both positively and negatively charged proteins in the nanocapillary.

In the experiments where the gated diffusive transport of proteins was investigated, one channel (source) was filled with a protein solution and the other (drain) was filled with 0.01× PBS. The source and drain electrodes were grounded throughout the experiments. Figure 4c presents a representative experiment in which the transport of negatively charged GFP was investigated. Initially, a gate voltage of −10 V was applied to achieve a negatively charged surface, and thus, the capillary was set to be cation-selective. In this state, the GFP molecules were electrostatically repelled from entering the capillary and

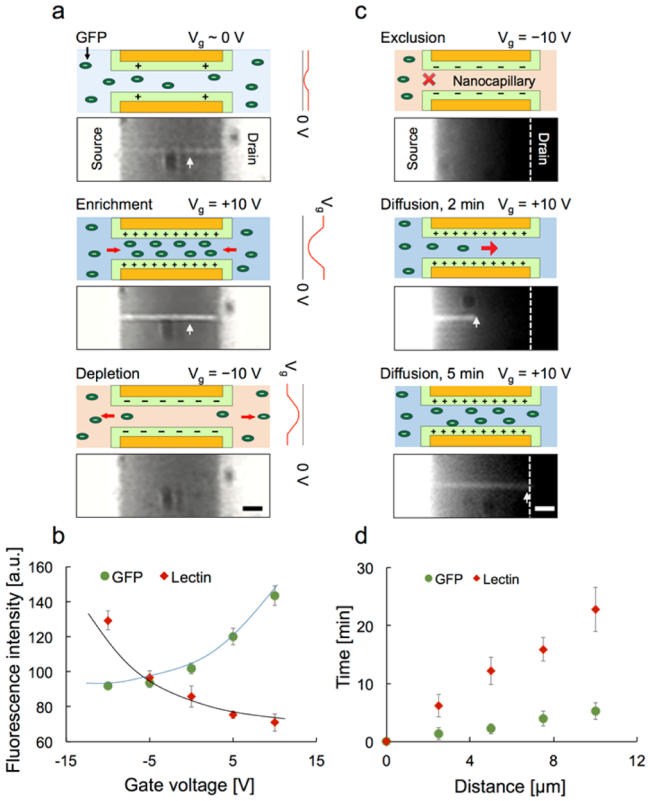

Figure 4. Field-effect regulation of protein transport under a zero source-to-drain bias. (a) Fluorescence micrographs showing the nanocapillary (arrows) with both ends exposed to equal concentrations of green fluorescent protein (GFP) at zero gate bias (top) and at either positive gate bias (GFP enrichment, middle) or negative gate bias (GFP depletion, bottom). In the schematic descriptions, the red curves denote the potential profile across the capillary for the corresponding gate bias with respect to the ground (gray lines). (b) Fluorescence intensity of the nanocapillary measured with GFP or lectin molecules (legend) and plotted as a function of the gate voltage. (c) Fluorescence images showing the gate control of GFP diffusion through the nanocapillary. The diffusive transport was suppressed under a negative gate bias at −10 V, and then was restored (arrows) upon switching to a positive gate bias at +10 V. (d) Migration distance *versus* diffusion time, measured for GFP and lectin molecules (legend). The background coloring denotes the ions that predominantly occupied the capillary: cations (pink) in (a) and anions (blue) in (c). Scale bars: 2 μm. Electrolyte condition: 0.01× PBS (~1.6 mM, pH 7.4).

the transport was hindered. This "off" state could persist over a long period (>1 h) without showing any noticeable change in the fluorescence intensity. However, GFP transport through the nanocapillary was no longer suppressed when the gate bias was switched to +10 V and the transistor was sent to an "on" state. The images show a fluorescent front (arrows) advancing and reaching the other end of the 10-μm-long nanocapillary in ~5 min. The control of the transport of the positively charged lectin was also demonstrated in an experiment in which a +10 V gate bias was applied to achieve the "off" state and a −10 V gate bias was used to allow the molecules to diffuse through the nanocapillary (Figure 4d); the lectin molecules were observed to diffuse inside the nanocapillary more slowly than GFP molecules, which is probably because the molecular weight of the lectin (~98 kDa) is higher than that of GFP (27 kDa). The effective diffusivity of these proteins was roughly estimated to

DOI: 10.1021/acsnano.6b00610
ACS Nano 2016, 10, 3985−3994

be $D_{GFP} \sim 3.4 \times 10^{-13}$ m^2/s and $D_{lectin} \sim 7.2 \times 10^{-14}$ m^2/s based on the ratio l^2/t, where l is the capillary length and t is the transport time. These values are approximately 2 orders of magnitude lower than those measured in free bulk solutions. A drastically lowered diffusivity of proteins in nanochannels has been described previously: Karnik *et al.* reported that the diffusivity of avidin in 30 nm nanochannels was roughly 2 orders of magnitude lower than that in the bulk solution.[20] Durand *et al.* reported that the effective diffusivity of wheat germ agglutinin in 50 nm slits was decreased by 4 orders of magnitude.[42] This phenomenon is considered to occur as a result of either the molecule−surface electrostatic interaction[20] or a dynamic adsorption−desorption of molecules on the surface[42,43] given the extremely high surface-area-to-volume ratio of the nanochannels.

Field-Effect Regulation of DNA Translocation. After validating the field-effect capacity of the nanocapillary-based NFET on the modulation of ionic conductance and protein transport, we investigated the device effectiveness for slowing DNA translocation under an appropriate gate bias. First, we detected single DNA translocation events by measuring the source-to-drain current without a gate bias. In the experiments, λ-phage DNA was dissolved to a final concentration of ∼8 μg/mL in 1 M KCl solution containing 10 mM Tris-borate (pH 8.0) and 1 mM EDTA. The DNA solution was loaded into both channels of a device featuring a 20-μm-long nanocapillary (l = 20 μm), and a 1 V source-to-drain bias was applied to electrophoretically drive the DNA chains while leaving the gate electrode floating. Figure 5a shows the ionic currents through the nanocapillary measured before and after the introduction of DNA. In the plots, the baseline current of ∼4 nA was subtracted. The results show that the ionic current exhibited frequent downward dips following the introduction of DNA, which was attributed to a DNA-associated ionic current blockage effect.[44] Further representative current traces are shown in Figure S5. In the following, it is argued that each current dip corresponds to the translocation of a single λ-DNA chain, which can be identified with a characteristic translocation time (Δt) and current blockage (ΔI) as defined in Figure 5a (inset).

In an optical experiment, the translocation of fluorescence-stained λ-DNA chains was observed under a floating gate and a 1 V source-to-drain bias (Supporting Information, Movie). A careful examination of the frames suggests that DNA coils were partially inserted into the capillary upon collision and then retracted under thermal fluctuations. These failed attempts were short-lived and far less assertive than a typical translocation event captured in the early frames. During the translocation event (Figure S6), the chain was trapped for a fraction of time until it overcame the entropic barrier and crossed the capillary; the total event duration registered was ≳2 ms and comparable to the most probable translocation time measured from the current dips (Figure 5b). Events below 1 ms were extremely rare (<1%) and dismissed as failed attempts risen above the noise level. It should be noted that the optical experiment had to be conducted at a lower ionic strength buffer (0.2 M KCl) than the stated above to avoid the quenching of fluorescence, which rendered the detection of the transient current blockades difficult. Nevertheless, neither EOF nor the translocation time was expected to vary because of the thin EDL ($\lambda_D \sim 1$ nm) and weak surface charge of alumina under a floating gate.

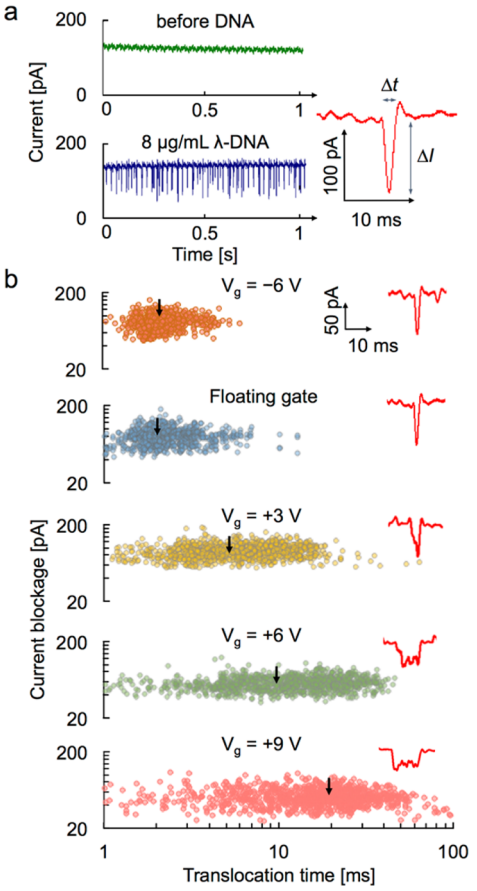

Figure 5. Field-effect regulation of DNA translocations with 1 M KCl buffer under a source-to-drain bias of 1 V. (a) Ionic currents measured in a set of comparative control experiments under a floating gate. The current exhibits frequent downward dips upon the introduction of λ-DNA prepared with 1 M KCl containing 10 mM Tris-borate (pH 8.0) and 1 mM EDTA. Inset: a representative current dip corresponding to a single DNA translocation event, characterized here by its translocation time (Δt) and current blockage (ΔI). (b) Event scatter plots of λ-DNA translocation time *versus* current blockage, each featuring 1000 single translocation events recorded under a specific gate bias. The arrows point at single events for which the corresponding current traces are shown (insets).

Notably, the frequency of the λ-DNA translocation events (∼31.2 Hz) in our device was considerably higher than the event frequency measured in 50 nm silica nanotubes (<1 Hz).[27] This high-throughput behavior probably originates from the positively charged surface of alumina, which electrostatically favors the translocation of negatively charged DNA chains.[45] Moreover, the positive surface charge, albeit weak, can induce an EOF, which is along the same direction as the electrophoretic driving force and unable to oppose the translocation of chains. The high-throughput behavior might at first suggest an increased likelihood of finding multiple chains in the capillary at a given time during a translocation event. This type of events, however, is hard to detect in our device based on a characteristic current dip profile, unlike in nanopores. So is the translocation of a single chain in a folding state, the ability to resolve instantaneous number of strands based on the quantized current levels is lost due to the extensive capillary length here. Nevertheless, since the translocation involves an insertion phase in which a coil is being trapped at the capillary

DOI: 10.1021/acsnano.6b00610
ACS Nano 2016, 10, 3985−3994

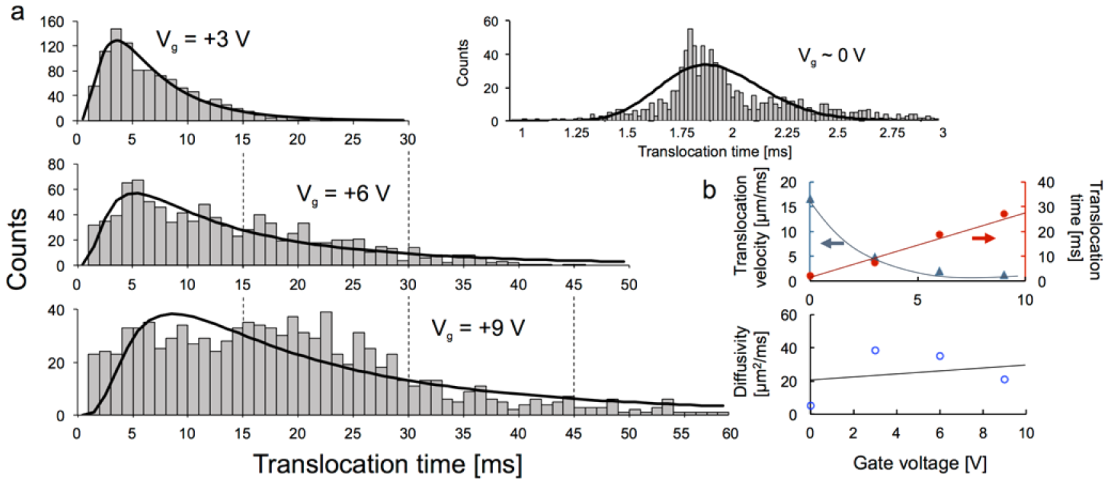

Figure 6. (a) Event histograms of λ-DNA translocation time measured under a set of distinct gate bias conditions. Respective fittings refer to a first passage time distribution derived from a simple 1D biased diffusion model. The unit interval (column width) is 0.02 ms for the floating gate (inset) and 1 ms for the positive gate voltages. (b) Translocation velocity (blue) characteristic translocation time (red), and diffusion constant, all plotted as a function of gate bias. Electrolyte condition is as stated in Figure 5.

entrance by an entropic barrier for a fraction of time comparable to Δt, the concurrent translocation of multiple chains is likely only if the chains happen to overcome the entropic barrier together, which seems to be unlikely. Therefore, each current dip is assumed to represent the translocation of a single λ-DNA.

To assess the extent of DNA translocation events that can be regulated in our device, we performed λ-DNA translocation experiments under various gate bias conditions: $V_g = -6$, ~0, +3, +6, and +9 V. The results showed that DNA translocation could be slowed under a positive gate bias, but that an applied negative gate bias ($V_g = -6$ V) exerted a negligible effect on DNA translocation in relation to a floating gate ($V_g \sim 0$ V). This is shown through event scatter plots (translocation time *versus* current blockage) in Figure 5b where each point corresponds to a single translocation event measured under a specific gate bias and each gate bias is represented by 1000 single translocation events. As can be seen, the translocation time under a positive gate bias was markedly increased in proportion with the gate bias strength. Intriguingly, this increase was accompanied by a proportionally increased variation of the translocation time across single events. Such increased variations were also observed with the passive methods proposed to reduce the translocation speed (*e.g.*, reduced electrophoretic drive, increased medium viscosity).[12,46]

To better visualize the spreading of the translocation time across single events, corresponding event histograms were constructed (Figure 6a). Each histogram was fitted using a recently developed 1D biased diffusion model for DNA translocation.[47,48] In the model, the distribution of DNA translocation time can be described by the first-passage probability density function,

$$F(\Delta t) = L/\sqrt{4\pi D \Delta t^3} \cdot e^{-(L-v\Delta t)^2/4Dt}$$

where v is the translocation velocity, D is the diffusion constant, and $L = l + L_{DNA}$ is the translocation length with L_{DNA} being the contour length of λ-DNA (~16 μm).[49] When the histograms were fitted with the model, the corresponding values of v and D were extracted. In addition, the characteristic translocation time (τ) was calculated from $\tau = L/v$ for each specific gate bias condition. The values of v and τ were plotted as a function of the applied gate bias in Figure 6b. As shown, v was ~18.4 μm/ms under a floating gate ($V_g \sim 0$), which corresponds to a rate of ~54.1 bp/μs given that each base pair of DNA has a length of 0.34 nm. When a gate voltage of 9 V was applied, v was decreased by over an order of magnitude down to ~1.33 μm/ms (3.9 bp/μs). This performance surpasses those of the passive methods; DNA translocation speed was decreased by ~5-fold with increased medium viscosity,[12] ~2-fold with lowered temperature or increased salt concentration,[12] and ~4-fold with altered pH.[50] More importantly, the results verify that the device is capable of providing dynamic and flexible regulation of the DNA translocation time by simply varying the gate bias.

The characteristic translocation time τ was observed to follow a nearly linear trend with the gate voltage, gradually increasing from ~1.9 to 27.1 ms as the gate bias was increased from $V_g \sim 0$ to 9 V. The D values (Figure 6b), however, appeared to be ~5 orders of magnitude higher than the diffusion constant in free solutions (~4.6×10^{-4} μm²/ms).[51] Intriguingly, the same model when applied to the electrophoretic translocation of 40 nm spheres through a triangular nanochannel (<500 nm in all three dimensions) showed good agreement with a theoretical value calculated for bulk Brownian diffusion.[52] Thus, the discrepancy here can be attributed in part to the conformational change of λ-DNA chains during the translocation and also the capillary high-aspect ratio (50 nm diameter and 20 μm length). Similar discrepancies were also noted for the diffusion constant obtained from the same model when it was applied to the DNA translocation measurements across nanopores: for double-stranded DNA coils (length, 2–23 kbp), the diffusion constant obtained was ~2 orders of magnitude larger than that in the bulk.[47,48] Li *et al.* argued that the discrepancy in D might originate from a more complicated translocation process than the 1D model assumes, as the segment of DNA must undergo uncoiling and recoiling.[47] Ling *et al.*, based on the obtained quadratic dependence of D on the driving voltage, argued that the increased D in nanopores can be considered as a consequence of a Taylor-dispersion effect due to a spatially nonuniform EOF velocity profile.[48] EOF was also held responsible for the reduced mobility of DNA extracted from the model since EOF in a silica nanopore is

DOI: 10.1021/acsnano.6b00610
ACS Nano 2016, 10, 3985–3994

against the electrophoresis direction. However, EOF in a capillary must display a spatially uniform velocity profile except in the vicinity of the capillary wall (<1 nm here). Rather, the translocation process here is further complicated by the entropic trapping of chains during their insertion into the capillary. This causes a certain delay depending on the driving field strength and the chain size as revealed by our recent studies on sieving DNA through a periodic arrangement of such capillaries.[33,34]

The effective slowing of DNA translocation speed under a positive gate bias has been predicted in previous theoretical studies: the induction of positive charge of the nanochannel surface can lead to a strong electrostatic attraction exerted on negatively charged polynucleotides at a distance shorter than the Debye screening lengths combined; this will attract the DNA to the surface and hence impose pronounced electrostatic interaction.[18,19] Notably, Ai *et al.* predicted that whereas a dominant DNA–nanopore electrostatic interaction can affect the translocation behavior under a low electric field drive (10 kV/m), the effect is negligible when the electric field drive is increased to 1 MV/m.[18] In our experiments, the field drive was low (~50 kV/m), so our findings agree with this theoretical prediction. However, the theoretical model considered only short DNA strands that were approximated as rigid nanorods. A comparatively more realistic model in which the stretching and the conformational variation of a DNA chain translocating across the nanochannel are considered for accurately estimating the translocation process in our device has not yet been developed. Meanwhile, Luan *et al.*, using all-atom molecular dynamics simulations, concluded that the DNA translocation under a field effect proceeds in "stick–slip" fashion,[53] depending on the axial and transversal field strengths and the DNA–nanopore surface interactions; when the thermal activation overcomes the electrostatic forces, DNA is temporarily released from the nanopore surface and then returned to the surface and immobilized again. The translocation of an elongated chain consists of such repeated stick and slip steps.

The extracted value of v was further used to calculate the frictional force. DNA chains driven under a floating gate (v = 18.4 μm/ms) were assumed experiencing only a hydrodynamic frictional force $f = n_0 L_{DNA} E/v$, where n_0 is the charge per unit length of λ-DNA (~1.4e/nm),[54] and E is the electric field strength. This resulted in a value of 10.8 nN·s/m, which is in good agreement with the previously reported value for λ-DNA (~7.6 nN·s/m).[49] However, the calculation of a contact friction under a positive gate bias is involved due to the nonequilibrium "stick–slip" motion. A gross estimation of such additional friction can be obtained from $F_{surface} = n_0 L_{DNA} E - fv$, and could be as high as ~180 pN under a gate bias of 9 V (v = 1.33 μm/ms), assuming f = 10.8 nN·s/m. For the applied gate bias to be effective, however, the DNA chain has to be nearly in contact with the capillary surface because of the thin EDL (λ_D ~ 0.3 nm) under the stated high-salt buffer (1 M KCl, 10 mM Tris-borate, pH 8.0, and 1 mM EDTA). Such "contact" sites might be dynamically created and removed through diffusion (the stick–slip motion) or during the restriction-induced conformational change of the DNA chain. This buffer condition was used in previous nanopore-based DNA detection experiments.[44,45] Under a low-salt condition (*e.g.*, 100 μM KCl), the ionic current signal would be otherwise too weak to be recovered from the background noise.

It is worthwhile to note that the effective reduction of DNA translocation speed in our device cannot be explained by the surface-charge-induced EOF, because the EOF in our device is along the same direction as the electrophoretic driving force given that the alumina surface is positively charged. Moreover, the EOF was overly suppressed under the high-salt condition. Thus, a strong positive gate bias can slow the DNA translocation in our device, which is unlike of previous theoretical studies suggesting the use of a negative gate bias based on the condition that EOF is the dominant retarding force.[18] Meanwhile, experimental studies have shown that, for single-stranded DNA, nanopore translocation dynamics greatly differ from those for double-stranded DNA;[55,56] a comparatively increased translocation speed and a reduced current blockade have been reported for the former.[55] Since single-stranded DNA is of great interest for nanopore sequencing, its capillary translocation dynamics shall be explored under an applied gate bias. These experiments could be conducted under alkaline pH or increased temperature to prevent the strand from becoming a blob, *i.e.*, hybridized into a random coil (assuming a long heteropolymer).[55] Under alkaline pH, however, the capillary exhibits an enhanced negative surface charge density (Figure 3b), and the subsequent EOF opposes the DNA translocation. Alternatively, experiments could be conducted under neutral pH in which case the highly entangled blob would have to face a greater barrier at the capillary entrance than double-stranded DNA of a comparable size; unraveling the blob during the capillary insertion would require breaking many hydrogen bonds.[56] Such enhanced barrier might allow for prolonged electrostatic interactions and a more pronounced field effect under a positive gate bias. Although the platform demonstrated here could be used for the field-effect probing of long polymer chains to study polymer dynamics, its application to nanopore sequencing would be of an utmost interest and call for a nanopore (in-plane) structure based on a process that is amenable to the nanocapillary integration. Such in-plane nanopore sensor is currently under development and will be reported in due course.

CONCLUSION

Slowing DNA translocation across a nanochannel by modulating the channel surface charge through an external gate bias has been experimentally demonstrated. This was achieved using a nanofluidic field effect transistor featuring a 50 nm-diameter in-plane alumina capillary that is surrounded by a gate electrode along its entire length. The device exhibits an ambipolar and pH-dependent characteristic owing to the effective gate configuration and the weak surface charge of alumina. Thus, the device can control the transport of both positively and negatively charged proteins. More importantly, the capillary surface under a positive gate bias imposes a strong electrostatic attraction on DNA chains and thus lowers the translocation speed of DNA by 1 order of magnitude. Given its robustness and facile fabrication process that is compatible with standard semiconductor manufacturing, the device can potentially be integrated with tunneling electrodes or nanopores to play a vital role in a high-throughput and cost-effective DNA sequencing.

MATERIALS AND METHODS

Device Fabrication. The device was fabricated using standard semiconductor manufacturing techniques. The fabrication process is detailed in Supporting Information, Figure S1.

DOI: 10.1021/acsnano.6b00610
ACS Nano 2016, 10, 3985–3994

Chemicals and Materials. Green fluorescent protein (GFP) was purified from GFP-overexpressing *Escherichia coli* by using chromatography columns. FITC-conjugated lectin from *Lens culinaris* was purchased from Sigma-Aldrich (St. Louis, MO). Previous work has confirmed that this fluorescent labeling does not change the electrical charge property of the lectin.[35] The proteins were dissolved in 0.01× phosphate-buffered saline (PBS, pH 7.4) to a final concentration of 10 μM. Double-stranded DNA fragments from bacteriophage lambda *cI857 Sam7* (λ-DNA, 48 kbp) were obtained from Sigma-Aldrich and were prepared at a final concentration of 8 μg/mL in a buffer solution containing 1 M KCl, 10 mM Tris-borate, and 1 mM EDTA (pH 8.0). For optical experiment, the buffer concentration was kept at 0.2 M KCl and DNA fragments were stained at a dye/base pair ratio of 1:10 using the intercalating dye YOYO-1 obtained from Thermo Fisher Scientific (Waltham, MA). In all preparations, the solution pH was adjusted using HCl and KOH.

Measurements. A slab of polydimethylsiloxane (PDMS, Sylgard 184, Dow Corning, Corp., Midland, MI) punched with access holes was secured on the fabricated device through surface activation under oxygen plasma. Two Ag/AgCl wire electrodes were placed into the respective access ports for source and drain bias. Ag wire was secured to the exposed gate contact pad through silver colloidal paste (Ted Pella, Inc., Redding, CA). The device was characterized in a Faraday cage by using a semiconductor parameter analyzer (4145B, Agilent Technologies, Santa Clara, CA). In protein experiments, voltages were applied using a DC voltage supply (PS280, Tektronix, Beaverton, OR). In DNA experiments, current traces were recorded from source and drain electrodes connected to a patch-clamp amplifier (EPC 10 USB, HEKA Elektronik, Lambrecht, Germany). Gate voltages were applied using Duracell AAA batteries to eliminate the power supply interference. The current signal was sampled at a rate of 200 000 1/s and filtered through a built-in low-pass Bessel filter (100 kHz) and a Butterworth filter (5 kHz). The measurements were taken in a Faraday cage to shield against electromagnetic interference. In optical experiment, the capillary translocation of stained DNA fragments was observed under an epifluorescence microscope (Eclipse, Nikon, Tokyo, Japan) equipped with a solid-state laser at 488 nm and a filter cube set suitable for the excitation and detection of sample bands (ex/em 492/520 nm). Time-series images were captured by EMCCD (iXon3 897, Andor).

Characterization of DNA Translocation Events. The recorded current traces were used for characterization without further processing. The current dips were identified using the "Quick Peaks" function in the software OriginPro 8.5.1 (OriginLab Corporation, Northampton, MA), in which the peak value (current blockage) and peak width (translocation time) can be readily obtained.

ASSOCIATED CONTENT

Supporting Information

The Supporting Information is available free of charge on the ACS Publications website at DOI: 10.1021/acsnano.6b00610.

Additional materials related to the fabrication process and theoretical modeling and figures (PDF)

Movie (AVI)

AUTHOR INFORMATION

Corresponding Author

*E-mail: eelyobas@ust.hk.

Notes

The authors declare no competing financial interest.

ACKNOWLEDGMENTS

This work was financially supported by the Research Grant Council of Hong Kong under Grant No. 623912.

REFERENCES

(1) Dekker, C. Solid-State Nanopores. *Nat. Nanotechnol.* **2007**, *2*, 209−215.

(2) Craighead, H. Future Lab-on-a-Chip Technologies for Interrogating Individual Molecules. *Nature* **2006**, *442*, 387−393.

(3) Karhanek, M.; Kemp, J. T.; Pourmand, N.; Davis, R. W.; Webb, C. D. Single DNA Molecule Detection Using Nanopipettes and Nanoparticles. *Nano Lett.* **2005**, *5*, 403−407.

(4) Firnkes, M.; Pedone, D.; Knezevic, J.; Doblinger, M.; Rant, U. Electrically Facilitated Translocations of Proteins through Silicon Nitride Nanopores: Conjoint and Competitive Action of Diffusion, Electrophoresis, and Electroosmosis. *Nano Lett.* **2010**, *10*, 2162−2167.

(5) Kowalczyk, S. W.; Hall, A. R.; Dekker, C. Detection of Local Protein Structures along DNA Using Solid-State Nanopores. *Nano Lett.* **2010**, *10*, 324−328.

(6) Lam, E. T.; Hastie, A.; Lin, C.; Ehrlich, D.; Das, S. K.; Austin, M. D.; Deshpande, P.; Cao, H.; Nagarajan, N.; Xiao, M.; et al. Genome Mapping on Nanochannel Arrays for Structural Variation Analysis and Sequence Assembly. *Nat. Biotechnol.* **2012**, *30*, 771−776.

(7) Reisner, W.; Larsen, N. B.; Silahtaroglu, A.; Kristensen, A.; Tommerup, N.; Tegenfeldt, J. O.; Flyvbjerg, H. Single-Molecule Denaturation Mapping of DNA in Nanofluidic Channels. *Proc. Natl. Acad. Sci. U. S. A.* **2010**, *107*, 13294−13299.

(8) Clarke, J.; Wu, H. C.; Jayasinghe, L.; Patel, A.; Reid, S.; Bayley, H. Continuous Base Identification for Single-Molecule Nanopore DNA Sequencing. *Nat. Nanotechnol.* **2009**, *4*, 265−270.

(9) Shendure, J.; Ji, H. L. Next-Generation DNA Sequencing. *Nat. Biotechnol.* **2008**, *26*, 1135−1145.

(10) Branton, D.; Deamer, D. W.; Marziali, A.; Bayley, H.; Benner, S. A.; Butler, T.; Di Ventra, M.; Garaj, S.; Hibbs, A.; Huang, X. H.; et al. The Potential and Challenges of Nanopore Sequencing. *Nat. Biotechnol.* **2008**, *26*, 1146−1153.

(11) Xie, P.; Xiong, Q.; Fang, Y.; Qing, Q.; Lieber, C. M. Local Electrical Potential Detection of DNA by Nanowire−Nanopore Sensors. *Nat. Nanotechnol.* **2012**, *7*, 119−125.

(12) Fologea, D.; Uplinger, J.; Thomas, B.; McNabb, D. S.; Li, J. L. Slowing DNA Translocation in a Solid-State Nanopore. *Nano Lett.* **2005**, *5*, 1734−1737.

(13) Ghosal, S. Effect of Salt Concentration on the Electrophoretic Speed of a Polyelectrolyte through a Nanopore. *Phys. Rev. Lett.* **2007**, *98*, 238104.

(14) Kim, Y. R.; Min, J.; Lee, I. H.; Kim, S.; Kim, A. G.; Kim, K.; Namkoong, K.; Ko, C. Nanopore Sensor for Fast Label-Free Detection of Short Double-Stranded DNAs. *Biosens. Bioelectron.* **2007**, *22*, 2926−2931.

(15) Trepagnier, E. H.; Radenovic, A.; Sivak, D.; Geissler, P.; Liphardt, J. Controlling DNA Capture and Propagation through Artificial Nanopores. *Nano Lett.* **2007**, *7*, 2824−2830.

(16) Tsutsui, M.; He, Y. H.; Furuhashi, M.; Rahong, S.; Taniguchi, M.; Kawai, T. Transverse Electric Field Dragging of DNA in a Nanochannel. *Sci. Rep.* **2012**, *2*, 394.

(17) He, Y. H.; Tsutsui, M.; Fan, C.; Taniguchi, M.; Kawai, T. Controlling DNA Translocation through Gate Modulation of Nanopore Wall Surface Charges. *ACS Nano* **2011**, *5*, 5509−5518.

(18) Ai, Y.; Liu, J.; Zhang, B. K.; Qian, S. Field Effect Regulation of DNA Translocation through a Nanopore. *Anal. Chem.* **2010**, *82*, 8217−8225.

(19) Jou, I. A.; Melnikov, D. V.; McKinney, C. R.; Gracheva, M. E. DNA Translocation through a Nanopore in a Single-Layered Doped Semiconductor Membrane. *Phys. Rev. E* **2012**, *86*, 061906.

(20) Karnik, R.; Castelino, K.; Majumdar, A. Field-Effect Control of Protein Transport in a Nanofluidic Transistor Circuit. *Appl. Phys. Lett.* **2006**, *88*, 123114.

(21) Karnik, R.; Fan, R.; Yue, M.; Li, D. Y.; Yang, P. D.; Majumdar, A. Electrostatic Control of Ions and Molecules in Nanofluidic Transistors. *Nano Lett.* **2005**, *5*, 943−948.

(22) Nam, S. W.; Lee, M. H.; Lee, S. H.; Lee, D. J.; Rossnagel, S. M.; Kim, K. B. Sub-10-nm Nanochannels by Self-Sealing and Self-Limiting Atomic Layer Deposition. *Nano Lett.* **2010**, *10*, 3324−3329.

DOI: 10.1021/acsnano.6b00610
ACS Nano 2016, 10, 3985−3994

(23) Shin, S.; Kim, B. S.; Song, J.; Lee, H.; Cho, H. H. A Facile Route for the Fabrication of Large-Scale Gate-All-Around Nanofluidic Field-Effect Transistors with Low Leakage Current. *Lab Chip* **2012**, *12*, 2568−2574.
(24) Nam, S. W.; Rooks, M. J.; Kim, K. B.; Rossnagel, S. M. Ionic Field Effect Transistors with Sub-10 nm Multiple Nanopores. *Nano Lett.* **2009**, *9*, 2044−2048.
(25) Lee, S. H.; Lee, H.; Jin, T.; Park, S.; Yoon, B. J.; Sung, G. Y.; Kim, K. B.; Kim, S. J. Sub-10 nm Transparent All-Around-Gated Ambipolar Ionic Field Effect Transistor. *Nanoscale* **2015**, *7*, 936−946.
(26) Paik, K.-H.; Liu, Y.; Tabard-Cossa, V.; Waugh, M. J.; Huber, D. E.; Provine, J.; Howe, R. T.; Dutton, R. W.; Davis, R. W. Control of DNA Capture by Nanofluidic Transistors. *ACS Nano* **2012**, *6*, 6767−6775.
(27) Fan, R.; Karnik, R.; Yue, M.; Li, D. Y.; Majumdar, A.; Yang, P. D. DNA Translocation in Inorganic Nanotubes. *Nano Lett.* **2005**, *5*, 1633−1637.
(28) Reisner, W.; Morton, K. J.; Riehn, R.; Wang, Y. M.; Yu, Z. N.; Rosen, M.; Sturm, J. C.; Chou, S. Y.; Frey, E.; Austin, R. H. Statics and Dynamics of Single DNA Molecules Confined in Nanochannels. *Phys. Rev. Lett.* **2005**, *94*, 196101.
(29) Mannion, J. T.; Reccius, C. H.; Cross, J. D.; Craighead, H. G. Conformational Analysis of Single DNA Molecules Undergoing Entropically Induced Motion in Nanochannels. *Biophys. J.* **2006**, *90*, 4538−4545.
(30) Storm, A. J.; Chen, J. H.; Zandbergen, H. W.; Dekker, C. Translocation of Double-Strand DNA through a Silicon Oxide Nanopore. *Phys. Rev. E* **2005**, *71*, 051903.
(31) Persson, F.; Utko, P.; Reisner, W.; Larsen, N. B.; Kristensen, A. Confinement Spectroscopy: Probing Single DNA Molecules with Tapered Nanochannels. *Nano Lett.* **2009**, *9*, 1382−1385.
(32) Liu, Y. F.; Yobas, L. Cylindrical Glass Nanocapillaries Patterned *via* Coarse Lithography (> 1 μm) for Biomicrofluidic Applications. *Biomicrofluidics* **2012**, *6*, 046502.
(33) Cao, Z.; Yobas, L. Fast DNA Sieving through Submicrometer Cylindrical Glass Capillary Matrix. *Anal. Chem.* **2014**, *86*, 737−743.
(34) Cao, Z.; Yobas, L. Gel-Free Electrophoresis of DNA and Proteins on Chips Featuring a 70 nm Capillary-Well Motif. *ACS Nano* **2015**, *9*, 427−435.
(35) Franks, G. V.; Gan, Y. Charging Behavior at the Alumina-Water Interface and Implications for Ceramic Processing. *J. Am. Ceram. Soc.* **2007**, *90*, 3373−3388.
(36) Huang, M.-J.; Mei, L.; Yeh, L.-H.; Qian, S. pH-Regulated Nanopore Conductance with Overlapped Electric Double Layers. *Electrochem. Commun.* **2015**, *55*, 60−63.
(37) Ma, Y.; Yeh, L.-H.; Lin, C.-Y.; Mei, L.; Qian, S. pH-Regulated Ionic Conductance in a Nanochannel with Overlapped Electric Double Layers. *Anal. Chem.* **2015**, *87*, 4508−4514.
(38) Stein, D.; Kruithof, M.; Dekker, C. Surface-Charge-Governed Ion Transport in Nanofluidic Channels. *Phys. Rev. Lett.* **2004**, *93*, 035901.
(39) Yeh, L.-H.; Ma, Y.; Xue, S.; Qian, S. Gate Manipulation of Ionic Conductance in a Nanochannel with Overlapped Electric Double Layers. *Sens. Actuators, B* **2015**, *215*, 266−271.
(40) Ma, Y.; Xue, S.; Hsu, S.-C.; Yeh, L.-H.; Qian, S.; Tan, H. Programmable Ionic Conductance in a pH-Regulated Gated Nanochannel. *Phys. Chem. Chem. Phys.* **2014**, *16*, 20138−20146.
(41) Jiang, Z.; Stein, D. Electrofluidic Gating of a Chemically Reactive Surface. *Langmuir* **2010**, *26*, 8161−8173.
(42) Durand, N. F. Y.; Bertsch, A.; Todorova, M.; Renaud, P. Direct Measurement of Effective Diffusion Coefficients in Nanochannels Using Steady-State Dispersion Effects. *Appl. Phys. Lett.* **2007**, *91*, 203106.
(43) Schoch, R. B.; Bertsch, A.; Renaud, P. pH-Controlled Diffusion of Proteins with Different pI Values Across a Nanochannel on a Chip. *Nano Lett.* **2006**, *6*, 543−547.
(44) Chen, P.; Gu, J. J.; Brandin, E.; Kim, Y. R.; Wang, Q.; Branton, D. Probing Single DNA Molecule Transport Using Fabricated Nanopores. *Nano Lett.* **2004**, *4*, 2293−2298.
(45) Chen, P.; Mitsui, T.; Farmer, D. B.; Golovchenko, J.; Gordon, R. G.; Branton, D. Atomic Layer Deposition to Fine-Tune the Surface Properties and Diameters of Fabricated Nanopores. *Nano Lett.* **2004**, *4*, 1333−1337.
(46) Lu, B.; Albertorio, F.; Hoogerheide, D. P.; Golovchenko, J. A. Origins and Consequences of Velocity Fluctuations during DNA Passage through a Nanopore. *Biophys. J.* **2011**, *101*, 70−79.
(47) Li, J. L.; Talaga, D. S. The Distribution of DNA Translocation Times in Solid-State Nanopores. *J. Phys.: Condens. Matter* **2010**, *22*, 454129.
(48) Ling, D. Y.; Ling, X. S. On the Distribution of DNA Translocation Times in Solid-State Nanopores: An Analysis Using Schrödinger's First-Passage-Time Theory. *J. Phys.: Condens. Matter* **2013**, *25*, 375102.
(49) Meiners, J. C.; Quake, S. R. Femtonewton Force Spectroscopy of Single Extended DNA Molecules. *Phys. Rev. Lett.* **2000**, *84*, 5014−5017.
(50) Anderson, B. N.; Muthukumar, M.; Meller, A. pH Tuning of DNA Translocation Time through Organically Functionalized Nanopores. *ACS Nano* **2013**, *7*, 1408−1414.
(51) Balducci, A.; Mao, P.; Han, J. Y.; Doyle, P. S. Double-Stranded DNA Diffusion in Slitlike Nanochannels. *Macromolecules* **2006**, *39*, 6273−6281.
(52) Angeli, E.; Volpe, A.; Fanzio, P.; Repetto, L.; Firpo, G.; Guida, P.; Savio, R. L.; Wanunu, M.; Valbusa, U. Simultaneous Electro-Optical Tracking for Nanoparticle Recognition and Counting. *Nano Lett.* **2015**, *15*, 5696−5701.
(53) Luan, B.; Wang, C.; Royyuru, A.; Stolovitzky, G. Controlling the Motion of DNA in a Nanochannel with Transversal Alternating Electric Voltages. *Nanotechnology* **2014**, *25*, 265101.
(54) Keyser, U. F.; Koeleman, B. N.; Van Dorp, S.; Krapf, D.; Smeets, R. M. M.; Lemay, S. G.; Dekker, N. H.; Dekker, C. Direct Force Measurements on DNA in a Solid-State Nanopore. *Nat. Phys.* **2006**, *2*, 473−477.
(55) Fologea, D.; Gershow, M.; Ledden, B.; McNabb, D. S.; Golovchenko, J. A.; Li, J. Detecting Single Stranded DNA with a Solid State Nanopore. *Nano Lett.* **2005**, *5*, 1905−1909.
(56) Kowalczyk, S. W.; Tuijtel, M. W.; Donkers, S. P.; Dekker, C. Unraveling Single-Stranded DNA in a Solid-State Nanopore. *Nano Lett.* **2010**, *10*, 1414−1420.

DOI: 10.1021/acsnano.6b00610
ACS Nano 2016, 10, 3985−3994